Title: Deep seismo-volcanic tremors constrain the magma supply from the mantle

Authors: Weifan Lu[1]*, Nikolai M. Shapiro[1], Oleg Melnik[2], Vladimir Lyakhovsky[3], Jannes Münchmeyer[4], Cyril Journeau[5], Jean Soubestre[1], Léonard Seydoux[6]

Affiliations:

[1]ISTerre, Université Grenoble Alpes, CNRS, Université Savoie Mont Blanc, IRD, Université Gustave Eiffel, Grenoble, France

[2]Department of Earth Sciences, University of Oxford, UK

[3]Geological Survey of Israel, Jerusalem, Israel

[4]GFZ Helmholtz Centre for Geosciences, Potsdam, Germany

[5]Earth and Planets Laboratory, Carnegie Institution for Science, Washington, DC, USA

[6]Institut de physique du globe de Paris, UMR CNRS, Université Paris-Cité, Paris, France

*Corresponding author. Email: Weifan Lu (lu.weifan@univ-grenoble-alpes.fr)

Abstract:
Volcanic eruptions are driven by magma supplied from the mantle, yet deep magmatic flux remains poorly constrained. Here we propose to quantify it based on deep seismic tremors. We adopt a model of tremor generation by rapid growth of gas bubbles in response to magma decompression and establish a physical relationship between the cumulative seismic moment and the volume of the ascending magma. By applying this approach to the Klyuchevskoy Volcanic Group in Kamchatka, we estimate the deep magma volumetric supply rate of the order of 1 km^3 per year which is consistent with the very high eruptive activity of these volcanoes. The proposed framework provides a new way to probe magma transport at depth and improves constraints on future volcanic activity and associated hazards.

Main Text:

A volcanic edifice seen at the surface of the Earth is only the "tip of the iceberg". Volcanoes originate at depths of tens to hundreds of kilometers beneath Earth's surface, where mantle rocks begin to melt when temperature, pressure, and volatile content reach favorable conditions, generating magma (*1*). This magma, together with dissolved volatiles such as H_2O and CO_2, is then transported upward into crustal magmatic systems. A part of this magma rising from the mantle is extruded at the surface of the Earth during volcanic eruptions. At the same time, a significant portion of initial magma remains stored within the crust, where it cools to form plutonic rocks (*2*). Therefore, the rate of magma supply and transport has a fundamental control on the processes of crustal formation and volcanism (*3*). Knowledge of this rate is necessary to understand the likelihood and possible strength of future eruptions and to evaluate the associated hazards (*2-4*).

Magma emplacement and volcanic output

Fig. 1 shows a schematic representation of the magma generation, transport, emplacement, and extrusion at volcanoes. The total magma generation rate Q_{tot} (considered here equivalent to the deep magma influx from the mantle) is decomposed in the sum of a magma intrusion rate Q_i and a magma extrusion rate Q_e (*4*). All these quantities are, in principle, variable in time. However, the exact time histories could be measured only for the magma extrusion rate $Q_e(t)$ and only during recent decades from observations of ongoing eruptions for some best monitored volcanoes. Maximum values of Q_e can exceed thousands or even millions of cubic meters per second during the strongest eruptions. Conversely, it is equal to zero during periods of volcanic quiescence. Longer past eruption histories are reconstructed from geological studies of their deposits, a method that has only very limited time resolution. The knowledge of the total deep magma supply rate, Q_{tot}, and of the rate of magma intrusion into the crust, Q_i, is much more uncertain because of the absence of direct observations of processes occurring deep below the Earth's surface.

Therefore, the different magmatic rates are rather characterized with their long-term averaged values: $\langle Q \rangle = \frac{1}{\Delta t}\int_{t-\Delta t/2}^{t+\Delta t/2} q(\tau)\, d\tau$, where Δt is a sufficiently long time interval (from centuries to hundreds of thousands of years, depending on the level of activity of the studied magmatic system). Such long-term averaged fluxes satisfy to a good approximation: $\langle Q_{tot} \rangle \approx \langle Q_i \rangle + \langle Q_e \rangle$.

To date, the long-term emplacement rates, $\langle Q_i \rangle$, have been estimated only for a few of the most active and well-studied volcanic systems, by dividing the estimated total volume of magma stored in the crust, V_i, by the total duration of volcanic activity at that system, Δt, so that $\langle Q_i \rangle = V_i/\Delta t$ (*4*). Both quantities in this ratio are highly uncertain. In particular, the volumes of magma intruded at depth are based on geophysical methods (gravity, seismology, magnetotellurics) whose results are often poorly constrained (*5-7*).

A key result derived from these approximate long-term estimates is the so-called intrusive-to-extrusive (plutonic/volcanic) ratio, defined as: $\langle Q_i \rangle / \langle Q_e \rangle$ (*4, 8, 9*). These ratios, estimated for different volcanoes, are typically larger than 1 with a tendency to increase to values around 10 for volcanoes built on top of thick continental crust. This result indicates that a major part of the magma generated in the mantle eventually accumulates in the crust, forming plutonic rocks. Therefore, the long-term total rate of the magma generation $\langle Q_{tot} \rangle$ might be on average an order of magnitude larger than the eruption volume rate observed at the surface.

These long-term average estimates are very useful for understanding magma generation at large spatial and temporal scales. However, they provide little information about the present-day dynamics of deep processes beneath volcanoes. For most volcanic systems, we do not know whether magma continues to be supplied from the mantle at present, at what rate, and whether this deep magma flux is time-stationary or intermittent. In this paper, we develop an approach to quantify the volumes of fresh and active magma in the vicinity of the crust-mantle boundary and to obtain a proxy to the present-day deep magma influx Q_{tot}.

Deep long-period volcanic seismicity

Key geophysical observations providing insights into the magma transport from the mantle are deep long-period (DLP) earthquakes (*10-19*) and tremors (*20-22*). Sources of this seismicity are located in the uppermost mantle and lower crust, i.e., in the vicinity of the Moho and their physical origin is thought to be related to magmatic processes. Some authors suggested that the DLP earthquakes can be generated within stagnated and cooling magma bodies, either by release of thermal stresses (*23*) or by repeated pressurization of volatiles exsolved through crystallization, a process known as "second boiling" (*15*). While such mechanisms may be valid for extinct volcanoes or stagnant magma bodies that are disconnected from the eruptive centers at the surface, they cannot explain the strong link observed between the DLP activity at depth and the reactivation or eruption of volcanoes at the surface (*10, 13, 17, 21*). Scenarios and models assuming the circulation of fresh magma in the deep parts of volcanic plumbing systems (*24-26*) are better suited to explain the origin of the DLP seismicity beneath active volcanoes. In this case, we can logically expect that the total seismic moment of the observed deep seismicity is related to the volume of deep intruded magma.

Linking volumes of magma and volcanic seismicity

The idea to estimate the volume of intruded magma in the upper crust from volcanic seismicity has previously been explored for swarms of volcano-tectonic earthquakes (*27*). This study established a simple empirical relationship between the cumulative seismic moment M_0^{cum} and the volume of intruded magma V_i:

$$logV_i = 0.77logM_0^{cum} - 6.32 \quad (1)$$

This relationship has been validated by comparing seismicity with erupted or intruded magma volumes in cases when estimations were available. They supplemented volcanic observations with relationships between injected volumes of water and seismicity in well-characterized cases of induced seismicity.

However, applying the empirical relationship (1) to observations of DLP seismicity results in a strong under-estimation of magma volumes intruded from the mantle (as discussed in the following section). Therefore, here we establish a relationship directly based on physical models of seismo-volcanic sources.

Focal mechanisms of DLP earthquakes are known to a contain significant volumetric component (*28, 29*). Therefore, we consider sources associated with changes of volumes of batches of magma. Geometry of typical magmatic intrusions like dyke and sills have a small aspect ratio and can be approximated by a tensile crack model (materials and methods). The associated change in volume dV can be related to the isotropic component of the seismic moment tensor (*30*). The scalar seismic moment M_0 with the isotropic component of a tensile crack is:

$$M_0 = KdV \quad (2)$$

where K is the medium bulk modulus (*25, 31*). Moreover, in this case, the isotropic and deviatoric scalar seismic moments are nearly equal to each other (*30*). For different intrusion geometries, equations should be corrected by a shape factor close to one (*32, 33*).

We consider two possible scenarios when seismic waves are generated by the injected magma. In the first one, the fresh magma is injected into the opening cracks very rapidly, and this process directly generates seismic waves. In this case, every pulse of seismic waves is emitted by an injected volume dV that can be estimated from the seismic moment based on equation (2). The total volume V_{tot} is the sum of all small injections and is computed from the cumulative seismic moment:

$$V_{tot} = \frac{M_0^{cum}}{K} \tag{3}$$

In the second scenario, the first boiling of magma near Moho is considered (*34*). The motion of magma is rather aseismic. At the same time, every batch of ascending magma of volume V_b contains dissolved gases and at some depth becomes oversaturated. When the fluid pressure within the batch reaches a critical threshold, a rapid nucleation and growth of gas bubbles can be triggered, leading to the generation of seismic waves (*25, 26)*. The scalar seismic moment associated with one batch M_0^b is still related to the its volume change equation (2). This volume change dV_b is in turn proportional to the magma pressure increase due to degassing dP :

$$dV_b = \frac{M_0^b}{K} = \frac{dPV_b}{K_m} \tag{4}$$

where K_m is the bulk modulus of the magma. We combine (2) and (4) to obtain an estimation of the batch volume:

$$V_b = \frac{K_m}{dP} dV_b = \frac{K_m}{dP}\frac{M_0^b}{K} \tag{5}$$

Parameters dP and K_m in equation (5) are relatively poorly constrained. Melnik et al. (*25*) demonstrated that dP is close (but does not exceed) to the magma over-saturation pressure ΔP. It's typical value is 40 MPa (*35, 36*) but it can be a few times smaller in a heterogeneous magma and under certain emplacement conditions (*37*). Silicate melts are more compressible than surrounding rocks and the ratio $\frac{K_m}{K}$ is of the order of tens of percent (*38*). However, the compressibility of a mixture of melt with growing gas bubbles is less well known. Therefore, in our study, we use the ratio $\gamma = \frac{K_m}{dP} = \frac{V_b}{dV_b}$ that has been determined numerically (*26*) for a sill exhibiting volumetric expansion caused by rapid gas bubble growth. The numerically constrained value is $\gamma \approx 650$ (material and methods).

Additional uncertainty in equation (5) arises from the fact that the total measured seismic moment may have other contributions in addition to the rapid magma degassing (materials and methods). We assume that every batch of ascending magma at some point exhibits a rapid bubble nucleation and emits seismic waves. The total volume of ascending magma can then be estimated by summing contribution from all individual seismic events and, therefore, related to the cumulative seismic moment:

$$V_{tot} = c\gamma \frac{M_0^{cum}}{K} \tag{6}$$

where c is a coefficient regrouping different poorly known parameters used in the moment and volume estimations (materials and methods). In the following we set it to $c = 1$ and consider that this can add an order of magnitude uncertainty in the final results. We then compare estimates of V_i obtained from equations (1), (3), and (6).

Klyuchevskoy volcanic group

For our study, we selected the Klyuchevskoy Volcanic Group (KVG) in Kamchatka, Russia, one of the largest and most active clusters of subduction-zone volcanoes in the world (*39*). Over the past 7000 years, the average volcanic output rate for the Klyuchevskoy volcano alone has been estimated to be approximately 0.04 km^3/year (*40, 41*). Considering that the KVG hosts other very large and active volcanoes (Bezymianny, Plosky Tolbachik, Ushkovsky; **Fig. 2A**), the overall rate of the volcanic group may approach 0.1 km^3/year, which is about one order of magnitude higher than the magma output rate at other arc volcanoes and is slightly smaller but comparable to the magma output rate of the Hawaiian volcanism (0.1–0.18 km^3/year) (*42*). In addition, the KVG is situated on top of the relatively thick Kamchatka crust (~35 km) (*43*). Therefore, we expect an elevated intrusive-to-extrusive ratio and thus an average magma generation rate $<Q_{tot}>$ up to 1 km^3/year.

The KVG seismic activity is also very intense, with a nearly constant occurrence of volcanic earthquakes and tremors (*21, 44, 45*) and, in particular, DLP seismicity (*17*) whose rate is the largest among all monitored volcanoes in the world. Most of the DLP sources are spatially clustered below the Klyuchevskoy volcano and in the vicinity of the Moho (**Fig. 2, B and C**), which coincides with a deep sub-crustal magmatic reservoir imaged by seismic tomography (*46*).

Analysis of data from the KISS seismic experiment

We use the data of the 2015–2016 "Klyuchevskoy Investigation - Seismic Structure of an Extraordinary Volcanic System" (KISS) experiment (*47*) providing dense station coverage (figs S1 and S2). The analysis of the KISS continuous data resulted in highly complete catalogs of seismic tremors (*21*) and volcanic earthquakes (*17*) containing large amounts of DLP events (**Fig. 2**).

We use these seismic catalogs to estimate respective cumulative seismic moments with a focus on the deeper part beneath Klyuchevskoy volcano (for the defined region, see materials and methods). For earthquakes, the scalar seismic moment M_0 for each event is computed with a reverse moment magnitude formula (*48*). We apply this reverse formula to the DLP cluster identified in the catalog (*17*) and then compute the cumulative seismic moment $M_0^{eq} = 4.8 \times 10^{14}\ N \cdot m$. This integration provides a reasonable estimate because the magnitude distribution of the Klyuchevskoy DLP earthquakes is not Gutenberg-Richter type but has a characteristic value of $M \approx 1.35$ (*17, 49*) well exceeding the detection threshold.

We select a volume that englobes most of deep (below 25 km) tremors sources from catalog (*21*). It is defined as a 10 km radius cylinder centered at the DLP earthquake cluster as indicated with thick red lines in **Fig. 2**. Seismic moments of tremors are estimated directly from continuous seismograms (*50, 51*) (see materials and methods, figs. S3 and S4). The respective cumulative value is estimated at $M_0^{tr} = 2.2 \times 10^{17}\ N \cdot m$. This value is subject to significant uncertainties due to the detection of tremors in the noisy seismograms and to the estimation of their seismic moment. Despite the mentioned uncertainties (see materials and methods, table S1), the overall moment release of deep seismic tremors clearly dominates the one of DLP earthquakes (about two orders of magnitude larger).

We then apply equations (1), (3), and (6) to these cumulative seismic moments to obtain different estimates of volumes of magma intruded from the mantle during the 11 months of the KISS experiment (see materials and methods). The results are shown in **Table 1**. Using the tremor catalog, which dominates the total moment release, the empirical relationship (*27*) and the co-seismic crack-opening model (*25*) yield $V_{tot} = 1.1 \times 10^{-2}\ km^3$ and $2.2 \times 10^{-3}\ km^3$, respectively — two orders of magnitude below the ~1 km³ expected from the long-term volcanic output rate and intrusive-to-extrusive ratio over the same period. In contrast, the rapid-degassing model (*25*) yields $V_{tot} = 1.4\ km^3$, consistent within an order of magnitude with this independent estimate. We therefore retain the degassing model as the interpretation that best reflects the physics of DLP seismo-genesis, while noting that equations (1) and (3) substantially underpredict the expected magma flux from the mantle.

Estimated magma supply from the mantle

Because the tremor moment release dominates the one from earthquakes by more than two orders of magnitude, we base our final interpretation on the tremor catalog (*21*) and the degassing model of seismic source (*25*). Time evolution of the cumulative seismic moment of tremors and of associated estimated magma volume shown in **Fig. 3** is highly intermittent. Nearly quiescent periods alternate with very intense episodes when involved magma volumes increase very rapidly during a few weeks or months, like those starting in December 2015 and April 2016. During some of these deep episodes, the apparent volumetric rate remains above 0.25 km^3/month (~100 m^3/s) (**Fig. 3**), which is comparable with peak values of magma extrusion rate observed during effusive basaltic eruptions at volcanoes like Hawaii, Piton de la Fournaise, or Tolbachik (*52-54*). A simple interpretation would be that the presented curve corresponds exactly to the time-dependent magma supply rate $Q_{tot}(t)$. This would imply that the bubble growth is triggered when a portion of fresh ascending magma reaches the depth of the critical pressure threshold that remains constant in time. However, we cannot exclude another possibility that the episodes of enhanced outgassing can be triggered by rapid depressurization of the whole transcrustal magmatic system (*13, 21*). Such pressure transients "from above" could occur during the 2016 eruption and the December 2015 unrest and explain the respective steps in cumulative moment and volume.

The possible pressure transients may cause the fluctuation of the depths of the critical pressure around some average value. Still, their effect should average out over a sufficiently long time. After such averaging, the overall volume of magma that reaches the bubble-growth threshold equals the volumes of magma supplied from below that has crossed the average "critical" depth. We consider that for the very active Klyuchevskoy system, averaging over nearly a year may be sufficient to obtain a rough estimation of the deep magma supply rate. Therefore, we divide the estimated total volume V_{tot} by the duration of the experiment and obtain an estimation of Q_{tot} at approximately 1.5 km^3 per year. This value is in approximate agreement with the prediction based on known magma extrusion rate and assumed intrusive-to-extrusive ratio.

While the estimates presented here are subject to one order of magnitude uncertainties (as described in previous paragraphs and materials and methods), our result is a first quantitative estimate of present-day deep magma flux from the mantle. Using deep volcanic tremors as a quantitative proxy for deep magmatic flux provides a new means for probing active magma transport and may improve constraints on volcanic activity and associated hazards.

Table 1. **Estimates of magma volumes intruded from the mantle.** Estimates of volumes (in km^3) of magma intruded from the mantle based on catalogs of DLP seismicity observed during 11 months of the KISS experiment beneath the Klyuchevskoy volcanic group and based on different moment-volume relationships. Uncertainties are described in materials and methods (table S1).

		Empirical (*27*) *equation (1)*	Co-seismic crack opening by magma *equation (3), K=100 GPa*	Rapid degassing (*25*) *equation (6), K=100GPa,* $\gamma = 650$, *c = 1*
Earthquakes	Seismic moment	$4.8 \times 10^{14}\, N \cdot m$		
	Magma volume	$9.6 \times 10^{-5}\, km^3$	$4.8 \times 10^{-6}\, km^3$	$3 \times 10^{-3}\, km^3$
Tremor	Seismic moment	$2.2 \times 10^{17}\, N \cdot m$		
	Magma volume	$1.1 \times 10^{-2}\, km^3$	$2.2 \times 10^{-3}\, km^3$	$1.4\, km^3$

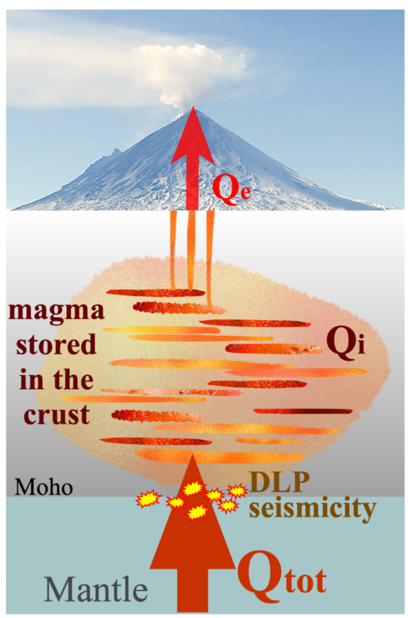

Fig. 1. Schematic representation of the magma generation, transport, emplacement, and output beneath volcanoes. Primary magmas are generated in the mantle and raise toward the surface through the crust where part of it is emplaced and forms plutonic rocks. Q_i is the rate of magma intrusion into the crust, Q_e is the magma extrusion rate, and Q_{tot} is the total rate of the magma generation (*4*). When averaged over sufficiently long time: $\langle Q_{tot} \rangle = \langle Q_i \rangle + \langle Q_e \rangle$. DLP earthquakes and tremors occurring near the crust mantle boundary are used in this study to track and to quantify the time dependent deep magma influx rate $Q_{tot}(t)$.

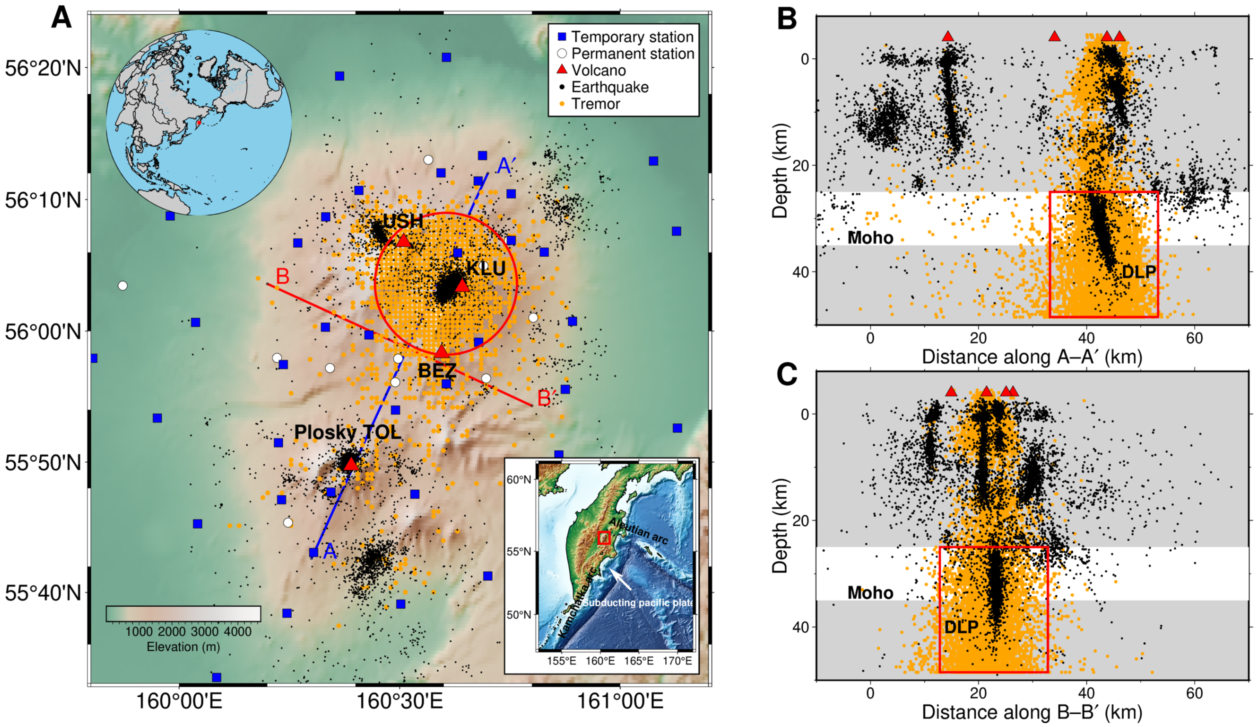

Fig. 2. Spatial distribution of seismicity, tremor activity, volcanic centers, and seismic stations in the Klyuchevskoy volcanic group. (A) Topographic map of the study area showing earthquake hypocenters (black circles) (*17*), tremor locations (orange circles) (*21*), active volcanoes (red triangles), permanent seismic stations (white circles), and temporary seismic stations deployed during the KISS experiment (blue squares). The blue and red lines denote the A–A′ and B–B′ profiles used for the vertical cross-sections shown in panels (B) and (C), respectively. The red circle outlines the selected tremor source region, defined as a cylindrical volume centered at 56.06°N, 160.605°E, with a radius of 10 km and a depth range of 25–48.5 km. Major volcanic edifices are labeled: Plosky Tolbachik (Plosky TOL), Bezymianny (BEZ), Ushkovsky (USH), and Klyuchevskoy (KLU). The upper-left inset shows the location of the study area within the northwestern Pacific region, whereas the lower-right inset illustrates the regional tectonic setting of Kamchatka and the Aleutian arc, including the direction of Pacific Plate subduction. **(B)** Vertical seismicity cross-section along profile A–A′. Earthquake hypocenters are shown as black dots and tremor locations as orange dots. Red triangles mark the projected positions of volcanic centers. The light-gray band denotes the approximate crust–mantle transition (Moho) at depths of ~25–35 km. **(C)** Vertical seismicity cross-section along profile B–B′. Symbols and annotations are the same as in panel (B).

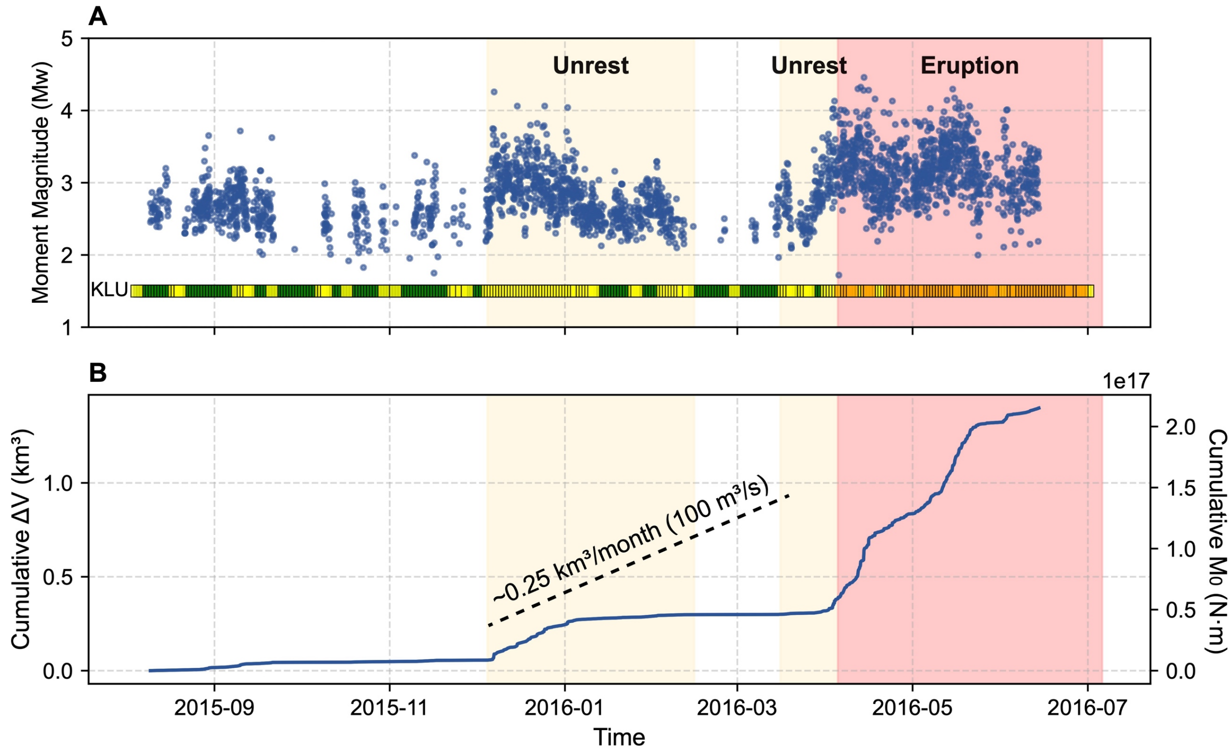

Fig. 3. Time dependent magma influx from the mantle $Q_{tot}(t)$ estimated from seismic tremors. (A) Moment magnitudes (M_w) of individual tremor events versus time. The horizontal color-coded bar at the bottom tracks the activity status of the Klyuchevskoy (KLU) volcano over the study period (*56,57*), where orange indicates an ongoing eruption. Shaded background regions mark periods of volcanic unrest (yellow) and active eruption (red). **(B)** Cumulative seismic moment release (M_0, right axis) and corresponding cumulative volume change (ΔV, left axis) estimated based on equation (6). Dashed line indicates the volumetric rate of 100 m^3/s, for reference.

References

1. B. Black, S. Naif, F. Horton, A. Goltz, C. Wilson, The deep frontier of mantle magma supply. *Eos* **106**, (2025).
2. H. Buurman, M. E. West, J. Power, M. Coombs, Seismic precursors to volcanic explosions during the 2006 eruption of Augustine Volcano. *The* **2006**, 41-57 (2006).
3. J. Claude, J.-C. Mareschal, A. Roman, The Formation of Continental Crust from a Physics Perspective. *Geochem. Int.* **56**, 1289-1321 (2018).
4. J. A. Crisp, Rates of magma emplacement and volcanic output. *Journal of Volcanology and Geothermal Research* **20**, 177-211 (1984).
5. J. O. S. Hammond, J. M. Kendall, Constraints on melt distribution from seismology: a case study in Ethiopia. *Geological Society, London, Special Publications* **420**, 127-147 (2016).
6. C. Magee *et al.*, Magma Plumbing Systems: A Geophysical Perspective. *J. Petrol.* **59**, 1217-1251 (2018).
7. M. Paulatto *et al.*, Advances in seismic imaging of magma and crystal mush. *Front. Earth Sci.* **Volume 10 - 2022**, (2022).
8. O. Bachmann, C. Huber, The volcanic/plutonic ratio in space and time, on Earth and beyond; How efficiently do magmas reach the surface during planetary evolution? *Lithos* **488-489**, 107825 (2024).
9. S. M. White, J. A. Crisp, F. J. Spera, Long-term volumetric eruption rates and magma budgets. *Geochemistry, Geophysics, Geosystems* **7**, (2006).
10. R. A. White, C. Newhall, R. Punongbayan, Precursory deep long-period earthquakes at Mount Pinatubo: Spatio-temporal link to a basalt trigger. *Fire and mud: Eruptions and lahars of Mount Pinatubo, Philippines*, 307-328 (1996).
11. J. A. Power, S. D. Stihler, R. A. White, S. C. Moran, Observations of deep long-period (DLP) seismic events beneath Aleutian arc volcanoes; 1989–2002. *Journal of Volcanology and Geothermal Research* **138**, 243-266 (2004).
12. M. L. Nichols, S. D. Malone, S. C. Moran, W. A. Thelen, J. E. Vidale, Deep long-period earthquakes beneath Washington and Oregon volcanoes. *Journal of Volcanology and Geothermal Research* **200**, 116-128 (2011).
13. N. M. Shapiro *et al.*, Deep and shallow long-period volcanic seismicity linked by fluid-pressure transfer. *Nature Geoscience* **10**, 442-445 (2017b).
14. M. Hensch *et al.*, Deep low-frequency earthquakes reveal ongoing magmatic recharge beneath Laacher See Volcano (Eifel, Germany). *Geophysical Journal International* **216**, 2025-2036 (2019).
15. A. G. Wech, W. A. Thelen, A. M. Thomas, Deep long-period earthquakes generated by second boiling beneath Mauna Kea volcano. *Science* **368**, 775-779 (2020).
16. Z. Song, Y. J. Tan, D. C. Roman, Deep Long-Period Earthquakes at Akutan Volcano From 2005 to 2017 Better Track Magma Influxes Compared to Volcano-Tectonic Earthquakes. *Geophysical Research Letters* **50**, e2022GL101987 (2023).
17. W. Lu, N. M. Shapiro, J. Münchmeyer, Magma Pathways Beneath the Klyuchevskoy Volcanic Group, Kamchatka, Revealed by a Machine-Learning-Based Earthquake Catalog. *Geophysical Research Letters* **53**, e2026GL123629 (2026).
18. R. Kurihara, K. Obara, Spatiotemporal Characteristics of Relocated Deep Low-Frequency Earthquakes Beneath 52 Volcanic Regions in Japan Over an Analysis Period of 14 Years and 9 Months. *Journal of Geophysical Research: Solid Earth* **126**, e2021JB022173 (2021).

19. N. M. Shapiro, J. Soubestre, C. Journeau, in *Modern Volcano Monitoring,* Z. Spica, C. Caudron, Eds. (Springer Nature Switzerland, Cham, 2025), pp. 107-146.
20. K. Aki, R. Koyanagi, Deep volcanic tremor and magma ascent mechanism under Kilauea, Hawaii. *Journal of Geophysical Research: Solid Earth* **86**, 7095-7109 (1981).
21. C. Journeau *et al.*, Seismic tremor reveals active trans-crustal magmatic system beneath Kamchatka volcanoes. *Science Advances* **8**, eabj1571 (2022).
22. J. Niu, X. Wang, M. Zhang, Q.-F. Chen, J. Jiang, Deep seismic tremor reveals trans-crustal fluid dynamics beneath Tengchong Volcano Field, Southwest China. *Journal of Volcanology and Geothermal Research* **473**, 108577 (2026).
23. N. Aso, V. C. Tsai, Cooling magma model for deep volcanic long-period earthquakes. *Journal of Geophysical Research: Solid Earth* **119**, 8442-8456 (2014).
24. M. Ukawa, M. Ohtake, A monochromatic earthquake suggesting deep-seated magmatic activity beneath the Izu-Ooshima Volcano, Japan. *Journal of Geophysical Research: Solid Earth* **92**, 12649-12663 (1987).
25. O. Melnik, V. Lyakhovsky, N. M. Shapiro, N. Galina, O. Bergal-Kuvikas, Deep long period volcanic earthquakes generated by degassing of volatile-rich basaltic magmas. *Nature Communications* **11**, 3918 (2020).
26. O. Melnik, V. Lyakhovsky, N. M. Shapiro, Rapid Gas Bubble Growth in Basaltic Magma as a Source of Deep Long Period Volcanic Earthquakes. *Journal of Geophysical Research: Solid Earth* **129**, e2024JB029602 (2024).
27. R. White, W. McCausland, Volcano-tectonic earthquakes: A new tool for estimating intrusive volumes and forecasting eruptions. *Journal of Volcanology and Geothermal Research* **309**, 139-155 (2016).
28. T. Ikegaya, M. Yamamoto, Spatio-temporal characteristics and focal mechanisms of deep low-frequency earthquakes beneath the Zao volcano, northeastern Japan. *Journal of Volcanology and Geothermal Research* **417**, 107321 (2021).
29. N. A. Galina, N. M. Shapiro, Source mechanisms of deep long period earthquakes beneath the Klyuchevskoy volcanic group (Kamchatka, Russia) inferred from S-to-P amplitude ratios. *Journal of Volcanology and Geothermal Research* **448**, 108049 (2024).
30. D. Bowers, J. A. Hudson, Defining the scalar moment of a seismic source with a general moment tensor. *Bulletin of the Seismological Society of America* **89**, 1390-1394 (1999).
31. K. Aki, P. G. Richards, *Quantitative Seismology*. (University Science Books, 2002).
32. A. McGarr, Seismic moments and volume changes. *Journal of Geophysical Research (1896-1977)* **81**, 1487-1494 (1976).
33. G. Müller, Volume Change of Seismic Sources from Moment Tensors. *Bulletin of the Seismological Society of America* **91**, 880-884 (2001).
34. K. F. McKee *et al.*, The plausible relationship between deep long-period earthquakes and volatiles: a case study of the Alaska-Aleutian arc. *Bull. Volcanol.* **88**, 115 (2026).
35. N. G. Lensky, R. W. Niebo, J. R. Holloway, V. Lyakhovsky, O. Navon, Bubble nucleation as a trigger for xenolith entrapment in mantle melts. *Earth and Planetary Science Letters* **245**, 278-288 (2006).
36. T. Shea, Bubble nucleation in magmas: A dominantly heterogeneous process? *Journal of Volcanology and Geothermal Research* **343**, 155-170 (2017).
37. O. Roche *et al.*, Shear-induced bubble nucleation in magmas. *Science* **390**, 633-637 (2025).
38. A. N. Clark, C. E. Lesher, Elastic properties of silicate melts: Implications for low velocity zones at the lithosphere-asthenosphere boundary. *Science Advances* **3**, e1701312.

39. N. M. Shapiro *et al.*, Understanding Kamchatka's extraordinary: Volcano Cluster. *EOS: Transactions, American Geophysical Union* **98**, 12-17 (2017a).
40. I. Melekestsev, Volcanism and relief formation. *Science, Moscow (in Russian)*, (1980).
41. S. Auer, I. Bindeman, P. Wallace, V. Ponomareva, M. Portnyagin, The origin of hydrous, high-δ18O voluminous volcanism: diverse oxygen isotope values and high magmatic water contents within the volcanic record of Klyuchevskoy volcano, Kamchatka, Russia. *Contrib. Mineral. Petrol.* **157**, 209-230 (2009).
42. V. Cayol, J. H. Dieterich, A. T. Okamura, A. Miklius, High Magma Storage Rates Before the 1983 Eruption of Kilauea, Hawaii. *Science* **288**, 2343-2346 (2000).
43. N. M. Shapiro, A. V. Gorbatov, E. Gordeev, J. Dominguez, Average shear-wave velocity structure of the Kamchatka peninsula from the dispersion of surface waves. *Earth, Planets and Space* **52**, 573-577 (2000).
44. S. Senyukov, Forecasting of the eruptions of volcanoes Klyuchevskoy and Bezymianny at Kamchatka. *Lambert Academic*, (2013).
45. D. V. Droznin *et al.*, Detecting and locating volcanic tremors on the Klyuchevskoy group of volcanoes (Kamchatka) based on correlations of continuous seismic records. *Geophysical Journal International* **203**, 1001-1010 (2015).
46. V. Levin, S. Droznina, M. Gavrilenko, M. J. Carr, S. Senyukov, Seismically active subcrustal magma source of the Klyuchevskoy volcano in Kamchatka, Russia. *Geology* **42**, 983-986 (2014).
47. N. Shapiro *et al.*, Klyuchevskoy volcanic group experiment (KISS). (2015).
48. T. C. Hanks, H. Kanamori, A moment magnitude scale. *Journal of Geophysical Research: Solid Earth* **84**, 2348-2350 (1979).
49. N. A. Galina *et al.*, Recurrence of Deep Long-Period Earthquakes beneath the Klyuchevskoi Volcano Group, Kamchatka. *Izvestiya, Physics of the Solid Earth* **56**, 749-761 (2020).
50. H. Kao, K. Wang, H. Dragert, J. Y. Kao, G. Rogers, Estimating seismic moment magnitude (Mw) of tremor bursts in northern Cascadia: Implications for the "seismic efficiency" of episodic tremor and slip. *Geophysical Research Letters* **37**, (2010).
51. J. B. Fletcher, A. McGarr, Moments, magnitudes, and radiated energies of non-volcanic tremor near Cholame, CA, from ground motion spectra at UPSAR. *Geophysical Research Letters* **38**, (2011).
52. S. M. Plank *et al.*, Estimates of lava discharge rate of 2018 Kīlauea Volcano, Hawaiʻi eruption using multi-sensor satellite and laboratory measurements. *Int. J. Remote Sens.* **42**, 1492 - 1511 (2021).
53. D. Coppola *et al.*, Thermal remote sensing reveals communication between volcanoes of the Klyuchevskoy Volcanic Group. *Scientific Reports* **11**, 13090 (2021).
54. A. Campus *et al.*, Effusion Rate Trends at Piton de la Fournaise: A Review of 24 Years of Space-Based Thermal Observation. *Journal of Geophysical Research: Solid Earth* **130**, e2024JB030962 (2025).
55. Kamchatka Branch of the Geophysical Survey of the Russian Academy of Sciences. (1961).
56. Daily activity level color codes for Kamchatka volcanoes (in Russian): www.emsd.ru/ssl/monitoring/main.htm/.
57. S. L. Senyukov, D. V. Droznin, I. N. Nuzhdina, S. Y. Droznina, The Twenty Five Years of "Volcanic Activity Monitoring"—Observations and Results. *J. Volcanol. Seismolog.* **20**, 284-304 (2026).

Acknowledgments: We thank Professor Han Yue for providing computational resources and acknowledge the High-Performance Computing Cluster of the Institute of Theoretical and Applied Geophysics, Peking University, for computational support.

Funding:

European Research Council under the European Union's Horizon Europe grant 101264310 DeepMagmaWaves (NS)

Author contributions:

Conceptualization: WL, NS

Methodology: WL, NS, OM, VL, JM, CJ, JS, LS

Investigation: WL, NS

Visualization: WL, NS

Funding acquisition: NS

Project administration: WL, NS

Supervision: NS

Writing – original draft: WL, NS

Writing – review & editing: WL, NS, OM, VL, JM, CJ, JS, LS

Competing interests: Authors declare that they have no competing interests

Data, code, and materials availability: KISS experiment data are available from the GEOFON datacenter at GFZ-Potsdam (KISS temporary stations (*47*); permanent stations: Kamchatka Branch of the Geophysical Survey of the Russian Academy of Sciences (*55*). The earthquake catalog and phase data generated in this study are available in (*17*). The tremor catalog in this study is available in (*21*).

Supplementary Materials

Materials and Methods

Figs. S1 to S6

Table S1

References (*58–65*)

Supplementary Materials for

Deep seismo-volcanic tremors constrain the magma supply from the mantle

Weifan Lu[1]*, Nikolai M. Shapiro[1], Oleg Melnik[2], Vladimir Lyakhovsky[3], Jannes Münchmeyer[4], Cyril Journeau[5], Jean Soubestre[1], Léonard Seydoux[6]

[1]ISTerre, Université Grenoble Alpes, CNRS, Université Savoie Mont Blanc, IRD, Université Gustave Eiffel, Grenoble, France

[2]Department of Earth Sciences, University of Oxford, UK

[3]Geological Survey of Israel, Jerusalem, Israel

[4]GFZ Helmholtz Centre for Geosciences, Potsdam, Germany

[5]Earth and Planets Laboratory, Carnegie Institution for Science, Washington, DC, USA

[6]Institut de physique du globe de Paris, UMR CNRS, Université Paris-Cité, Paris, France

Corresponding author: Weifan Lu (lu.weifan@univ-grenoble-alpes.fr)

The PDF file includes:

Materials and Methods

Data set

In this study, we used continuous three-component seismic records from the temporarily deployed KISS network (*39,47*), together with the permanent seismic network operated by the Kamchatkan Branch of the Geophysical Survey of the Russian Academy of Sciences (KBGS) (*55*) (Fig. S1). The KISS deployment lasted for 11 months, from August 2015 to July 2016 (Fig. S2). After quality control, we retained a final network of 101 stations for analysis.

Earthquakes and tremor catalogs

The earthquake catalog (*17*) was obtained with using a machine-learning–based detection workflow applied to data from the KISS seismic experiment in 2015–2016. The tremor catalog (*21*) was derived from the same data following the detection algorithm based on the network covariance matrix (*19, 58-61*). This approach analyzes the ensemble of cross-correlations between stations in the Fourier domain to extract coherent seismic signals from background noise. The initial catalog was generated by processing 44,020 windows, each 20 minutes in duration with a 50% overlap. By evaluating three network-based characteristic functions, 13,027 windows were successfully identified as long-period (LP) tremors or seismic swarms. To address the overlap inherent in the initial tremor detection windows, we implemented a merging criterion: subsequent tremor windows falling within the timeframe of a preceding window were consolidated into a single continuous event.

Furthermore, to focus specifically on the dynamics of the deep magmatic system, we constrained our analysis to tremors located beneath the Klyuchevskoy volcano, within a cylindrical volume centered at 56.06°N, 160.605°E, with a radius of 10 km and depths ranging from 25 to 48.5 km, as shown in Fig. 2B and 2C. The final dataset comprises 2494 distinct tremor events, with individual durations ranging from 20 to 360 minutes.

Theoretical framework and physical hypotheses

We consider that the DLP seismicity beneath the Klyuchevskoy volcanic group is dominantly generated by the mechanisms involving the rapid gas bubble growth in batches of over-saturated magma (*25,26*). Every batch of magma undergoing such seismogenic processes generates a pulse of seismic waves that are recorded as impulsive earthquakes or nearly continuous tremors for sources that are isolated or overlapped in time, respectively. We consider crack-shaped batches of magma embedded in the elastic rock. The magma is characterized by its bulk modulus K_m and the surrounding rock by the Lame parameters λ and μ with the rock bulk modulus being $K = \lambda + \frac{2}{3}\mu$. Seismic moment tensor associated with the crack volume change dV is (*31*):

$$M = \begin{bmatrix} \lambda dV & 0 & 0 \\ 0 & \lambda dV & 0 \\ 0 & 0 & (\lambda + 2\mu)dV \end{bmatrix} = \begin{bmatrix} m1 & 0 & 0 \\ 0 & m2 & 0 \\ 0 & 0 & m3 \end{bmatrix} \qquad (S1)$$

Associated isotropic and deviatoric scalar moments (*30*) are:

$$M_{ISO} = \frac{m1 + m2 + m3}{3} = \left(\lambda + \tfrac{2}{3}\mu\right) dV = KdV \qquad (S2)$$

$$M_{DEV} = \max(m1, m2, m3) - M_{ISO} = \tfrac{4}{3}\mu dV \qquad (S3)$$

For media with $\lambda = \mu$:

$$\frac{M_{ISO}}{M_{DEV}} = \frac{5}{4} \quad \rightarrow \quad M_{ISO} \approx M_{DEV} \qquad (S4)$$

The volumetric expansion of the magma can be related to the pressure change via its bulk modulus:

$$d\mathrm{P} = \frac{dV\, K_m}{V} \qquad d\mathrm{V} = \frac{dP\, V}{K_m} \qquad (S5)$$

Based on this, we can estimate magma volume from the scalar seismic moment:

$$V = \frac{K_m}{dP}\frac{M_{ISO}}{K} \approx \frac{K_m}{dP}\frac{M_{DEV}}{K} \qquad (S6)$$

We introduce a coefficient γ characterizing the degree of the magma expansion:

$$\gamma = \frac{K_m}{dP} = \frac{V}{dV} \qquad (S7)$$

and calibrate it based on numerical computation (*26*). This study considered rapid bubble growth within a 50 m radius and 3 m thick sills containing magma oversaturated at ΔP=40 MPa (*35, 36*). The volume change was estimated close to 36 m^3 resulting to estimation: $\gamma \approx 650$.

Estimation of the seismic moment of tremors

To estimate the seismic moment from volcanic tremor episodes, we implement a methodology based on the stochastic accumulation of small-scale source events (*50,51*). This approach allows for the quantification of long-duration signals that lack the discrete phases of typical earthquakes. Given the non-impulsive nature of these signals, the tremor is conceptualized as the continuous superposition of numerous independent, small-scale seismic sources. We assume that each infinitesimal segment of the recorded tremor signal is dominated by ballistic S-wave energy originating from a single discrete source. This allows for the application of standard S-wave propagation theory and radiation patterns.

Estimation of station noise levels

Because the noise level can vary substantially among stations and with time, background noise may bias the amplitude estimates of small-scale seismic signals. To account for this effect, we estimated the daily noise level for each station and each component separately.

For each station–component pair, we first excluded time periods containing identified tremors and DLP earthquakes. The remaining continuous waveform data were then divided into non-overlapping 5-s windows. For each window and at every station and component (Z, N, E), we calculated the root-mean-square (RMS) amplitude as a measure of the background noise level. The median RMS amplitude across all available 5-s windows was then used as the representative daily noise level for that station and component.

Data pre-processing and spectral characterization

Continuous three-component waveforms from the KISS and KBGS networks are first corrected for instrument response to obtain ground displacement. The analysis follows a modular workflow (Fig S3):

1. Temporal Segmentation: Following event detection from the tremor catalog, the signal is partitioned into short, non-overlapping sub-windows ($j = 1, \dots, J$) with a fixed duration of 5 seconds.
2. Noise-Level Screening: Only sub-windows with RMS amplitudes greater than twice the corresponding station- and component-specific daily noise level were retained for further analysis.
3. Frequency Domain Analysis: For each sub-window, a Fast Fourier Transform (FFT) is performed to evaluate the displacement spectrum.
4. Amplitude Extraction: The spectral displacement plateau, Ω_0, is defined as the median amplitude within the 1–5 Hz frequency band (Fig S4). This frequency range is selected to capture the primary energy of the DLP seismicity characteristic of the Klyuchevskoy volcanic system (*13,17,21*).

Seismic moment quantification

The scalar seismic moment at for an individual sub-window j at station i and component $comp$ ($M_{0,j}^{i,comp}$) is estimated by assuming a point source in a homogeneous half-space. We assume that each source is characterized by a "tensile crack" seismic moment tensor (S1) and, therefore, emits dominantly S-waves. Therefore, we use a simple Green's function for a far-field S-wave in a homogeneous infinite medium (*31*) and incorporate a correction for free-surface effects. We estimate the displacement amplitudes in a spectral domain and relate them to seismic moment as:

$$M_{0,j}^{i,comp} = \frac{4\pi\rho\beta^3 D(\Omega_{0,j}^{i,comp} e^{\frac{\pi f D}{Q\beta}})}{F \cdot R_{\theta\phi}} \qquad (S8)$$

Where ρ represents the medium density, taken as 2830 kg/m^3 (typical crustal value) (*62*); β is the S-wave velocity, set to 3500 m/s (*63,64*). D denotes the hypocentral distance between the tremor source and the recording station; $\Omega_{0,j}^{i,comp}$ is the median spectral displacement amplitude within the 1-5 Hz frequency band; F is the free-surface correction factor, assigned a value of 2.0; $R_{\theta\phi}$ is the average S-wave radiation pattern, taken as 0.72 (tensile crack mechanism) (*65*). Q is the quality factor describing anelastic attenuation of seismic waves, estimated at 86 as explained in the next section. The characteristic frequency was set to $f = 3$ Hz, corresponding to the center of the 1–5 Hz analysis band.

The total seismic moment for a specific component at a given station is then obtained by the linear summation of all sub-window moments over the total event duration:

$$M_{0,i}^{(comp)} = \sum_{j=1}^{J} M_{0,j}^{i,comp} \qquad (S9)$$

Seismic moment estimated from equation (S8) based on S-wave radiation characterizes mostly the deviatoric part of the focal mechanism. However, for a tensile crack the deviatoric and isotropic parts being nearly of the same strength (equations S4 and S6), the obtained estimates can be used to deduce the associated volume changes.

Estimation of cumulative magma volume

To derive a robust estimate of the total seismic moment (M_0) for a tremor episode, we take the median value of the total moments calculated across all available stations and components:

$$M_0 = median\left(M_{0,i}^{(E)}, M_{0,i}^{(N)}, M_{0,i}^{(Z)}, \dots, M_{0,M}^{(Z)}\right) \qquad (S10)$$

This statistical approach mitigates the influence of local site effects and varying signal-to-noise ratios across the network. The cumulative seismic moment $M_0^{cum}(t)$ is then computed as cumulative sum of scalar moments for individual tremor episodes.

Uncertainties in seismic moment to volume conversion

Following equations (S6) and (S7), the total magma volume V of magma exhibited a rapid outgassing is estimated from the cumulated seismic moment as:

$$\mathrm{V} = \gamma \frac{M_0^{cum}}{K} \qquad (S11)$$

Using the exact form of equation (S11) would imply that: (1) the whole recorded seismic signal is caused entirely by the gas bubble growth, (2) the geometry of tremor emitting magma batches is a pure tensile crack, and (3) every outgassing magma batch is initially oversaturated at 40 MPa, as in numerical simulations (*26*). Below we describe the uncertainties associated with these assumptions.

(1) The scalar seismic moment is estimated from the measured spectral displacement amplitudes Ω_0 (equation S8) that can be generated by multiple mechanisms including those not related to gas bubble growth (injection of new magma, friction of moving magma, fracturing of surrounding rocks …). Therefore, the part of the displacement due to the gas bubble growth and the related seismic moment represent only a portion of the total measured values:

$$\Omega_0^{bubble} = \xi \Omega_0, \quad M_0^{bubble} = \xi M_0 \qquad \text{(S12)}$$

where ξ is a correction coefficient smaller than one.

(2) For arbitrary magma batches geometries, equation (2) needs to be corrected with a shape factor θ close to one (*32,33*):

$$M_0^{bubble} = \theta K dV \qquad (S13)$$

(3) Considering a magma oversaturation different from the "tabular" value $\Delta P = 40MPa$ would result in a different amount of the volume change and of the associated coefficient γ. It should be replaced with some effective coefficient:

$$\tilde{\gamma} = \varphi \gamma \qquad (S14)$$

where φ is a correction coefficient. Considering that the oversaturation pressure can be reduced in a heterogeneous magma and under certain emplacement conditions (*37*), we expect those coefficient being smaller than 1 (up to a few tens of percent).

Combining all uncertainties results in:

$$V_{tot} = \frac{\xi}{\theta\varphi}\gamma\frac{M_0^{cum}}{K} \qquad (S15)$$

or in equation (6) with $c = \frac{\xi}{\theta\varphi}$. Considering that: $\xi < 1$, $\frac{1}{\varphi} > 1$, $\theta \approx 1$, we can expect that the overall correction coefficient c equals to one within an order of magnitude.

<u>Sensitivity of the cumulative seismic moment and magma volume estimates to model parameters and to source selection</u>

We assessed the sensitivity of the cumulative magma volume inferred from tremor seismic moments to the parameters used in the source and propagation corrections (Table S1). Ten alternative parameter combinations (C1–C9) were tested by varying the density, shear-wave velocity, quality factor, dominant frequency, analysis-window length, and medium bulk modulus, while keeping the remaining parameters fixed. These parameters affect either the estimated tremor seismic moment or its conversion to volumetric change in the rapid-degassing model. The reference model uses a depth range of 25–48.5 km, density of 2830 kg/m^3, shear-wave velocity of 3500 m/s, Q=95, dominant frequency of 3 Hz, a 5-s analysis window, and a pressure change of 40 MPa, consistent with the physical model adopted in the main text.

Another source of uncertainties is that the tremor sources are distributed over a large range of depths: 25-48.5 km (**Fig. 2**). In this configuration, we cannot exclude the possibility that, when being unsteadily transported over 25 km, a batch of magma may exhibit more than one episode of seismogenic bubble nucleation and that regrouping volume estimates from all possible sources may result in counting particular magma batches multiple times leading to overall volume overestimation. Therefore, we test the final results with different depth range of selected tremors sources (Fig. S5, Table S1).

The resulting cumulative volume estimates range from 0.5 to 3.0 km^3, compared with 1.4 km^3 for the reference model (Table S1). The largest variations are associated with the assumed source-depth range and pressure change, reflecting their direct influence on attenuation correction and on the conversion of seismic moment into volume change, respectively. Variations in density, shear-wave velocity, Q, frequency, and analysis-window length produce comparatively smaller changes.

Despite these parameter variations, the inferred cumulative volumes remain within the same order of magnitude. This sensitivity analysis therefore does not affect our principal interpretation that the observed deep tremor moment release represents substantial magma intrusion from the mantle. Rather, it indicates that the principal uncertainty is in the absolute magnitude of the inferred volume, consistent with our estimate being accurate primarily to an order of magnitude.

<u>Estimation of inelastic attenuation and quality factor Q</u>

We first estimated the seismic moment M_e for each station–event observation under the assumption of negligible inelastic attenuation by setting *Q=inf* in equation (S8). In this initial calculation, no attenuation correction was therefore applied to the observed spectral amplitudes. The resulting station-based moment estimates, $M_e^{station}$ show a systematic decrease with increasing hypocentral distance (Fig. S6), indicating that the assumption of *Q=inf* does not adequately account for the distance-dependent loss of seismic-wave amplitude.

To obtain an event-level reference moment that is minimally affected by attenuation, we first selected observations within a reference hypocentral distance of 70 km and retained only station estimates with $log_{10}\ M_e$ > 12. For each event, the initial event moment was then estimated as the median of the available near-distance station estimates, provided that at least three stations were available. This median-based procedure was adopted to reduce the influence of individual anomalous station measurements and to provide a robust event reference for the subsequent attenuation analysis.

For each station–event observation, we calculated the normalized seismic-moment residual as

$$\Delta log_{10}\ M_e = log_{10} M_e^{station} - log_{10} M_e^{event} \qquad (S16)$$

where M_e^{event} is the initial event moment estimated from the near-distance observations. This normalization substantially reduces the event-to-event variation in absolute seismic moment and isolates the systematic distance dependence of the station-based moment estimates. Thus, the residual $\Delta log_{10}\ M_e$ provides a measure of the apparent moment loss that remains when the spectra are processed assuming *Q=inf*.

We parameterized this distance dependence using a linear relation,

$$\Delta log_{10}\ M_e = a + br \qquad (S17)$$

where r is the hypocentral distance in kilometers, a is the intercept, and b is the distance-dependent attenuation slope. A negative value of b indicates that the seismic moment inferred without attenuation correction decreases systematically with increasing distance. In the present implementation, the attenuation coefficient was estimated using the linear estimator.

The physical basis for converting the fitted slope into an effective quality factor follows from the assumed exponential amplitude attenuation,

$$A(r) \propto \exp\left[-\frac{\pi f r}{Q\beta}\right] \qquad (S18)$$

where f is the representative frequency and β is the shear-wave velocity. Because the moment estimate derived from the uncorrected spectrum is proportional to the corresponding spectral amplitude, the logarithm of the apparent station moment is expected to decrease approximately linearly with distance:

$$log_{10} M_e^{station} - log_{10} M_e^{event} = C - \frac{\pi f}{Q\beta ln10} r \qquad (S19)$$

where C contains the distance-independent terms represented by the fitted intercept. Comparing with equation (S16) and giving:

$$b = \frac{\pi f}{Q\beta ln10} \qquad (S20)$$

And hence,

$$Q = \frac{\pi f}{-b\beta ln10} \qquad (S21)$$

This is the exact expression implemented in our analysis code. The calculation uses a reference frequency of f=3.0 Hz and a shear-wave velocity of $\beta = 3500\ m/s$. For the data shown in Fig. S6, the fitted relation has a negative slope, corresponding to an effective quality factor of approximately Q = 95.

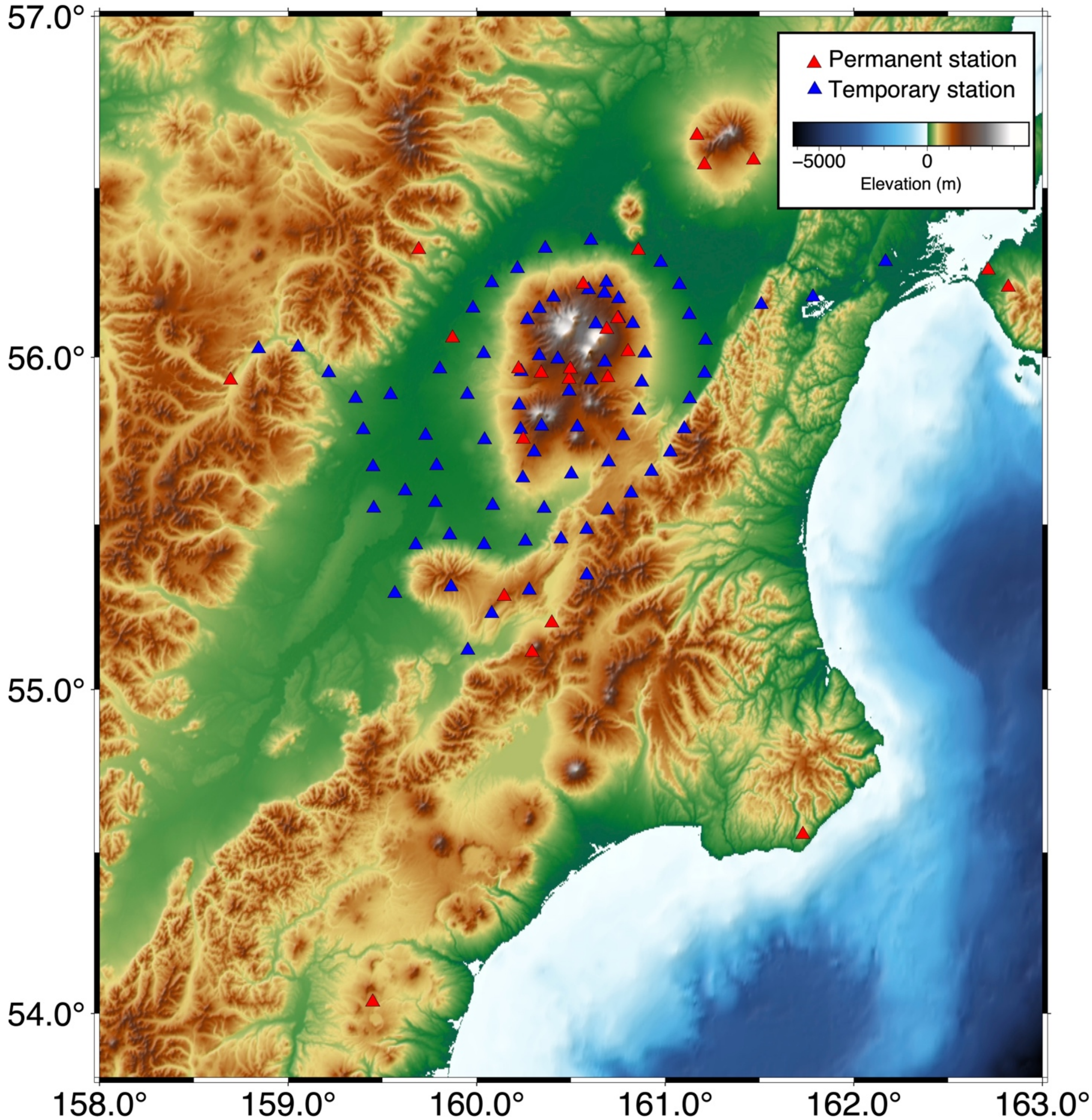

Fig. S1. Geographic distribution of seismic stations during the KISS experiment. Blue triangles represent temporary stations (network code X9), while red triangles indicate permanent stations (network code D0).

Fig. S2. Data availability of the seismic network. Timelines show the operational periods for individual stations within (a) the temporary X9 network and (b) the permanent D0 network from August 2015 to July 2016. Horizontal blue bars represent periods of continuous data recording.

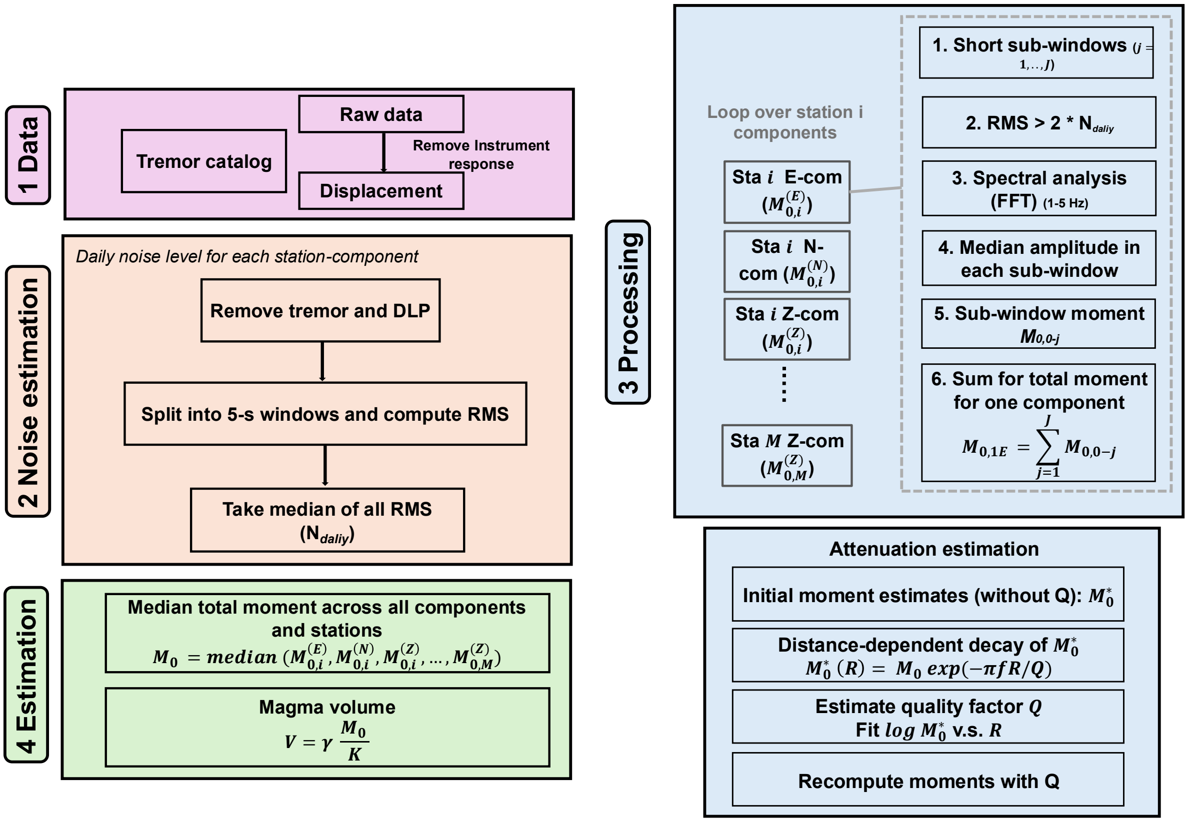

Fig. S3. Flowchart of the data processing pipeline. The workflow consists of four main stages: raw displacement data preparation and tremor filtering, daily noise level calculation, component-wise seismic moment calculation with attenuation correction via short-window spectral analysis, and final magma volume estimation based on the median seismic moment across all station components and gas overpressure.

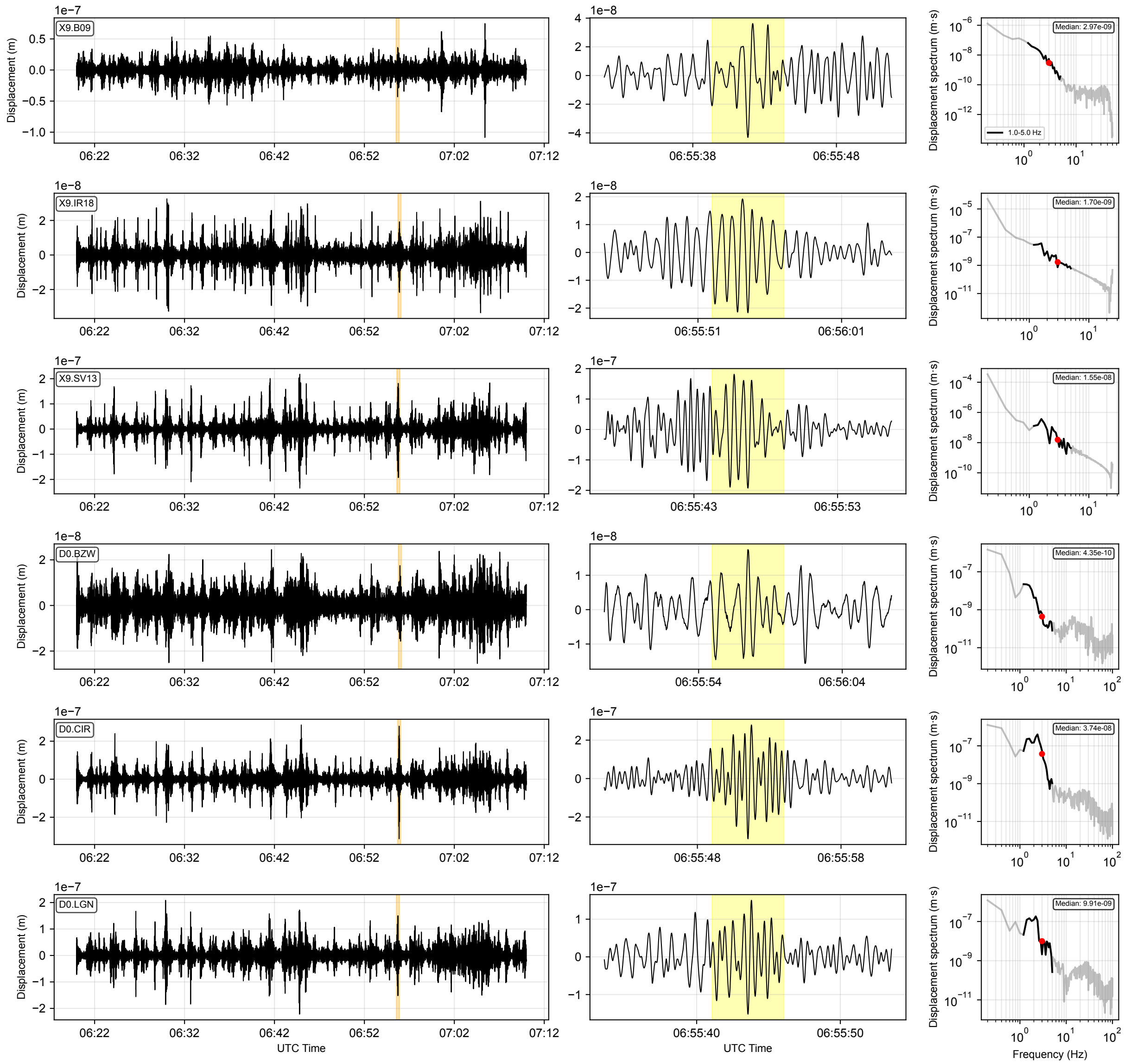

Fig. S4. Example of waveform processing and spectral measurement for a tremor event. The event occurred on 2016-03-27 at 06:20:00 UTC, located at 56.085°N, 160.577°E, with a focal depth of 46.5 km. A 50-minute tremor window starting at the origin time was analyzed. Left panels: displacement seismograms (vertical component) from six stations, with the target time window highlighted in orange. Middle panels: zoomed-in views of the selected window, with sub-windows shaded in yellow. Right panels: corresponding displacement amplitude spectra (black lines); red dots indicate the median spectral amplitudes computed within the 1.0–5.0 Hz band.

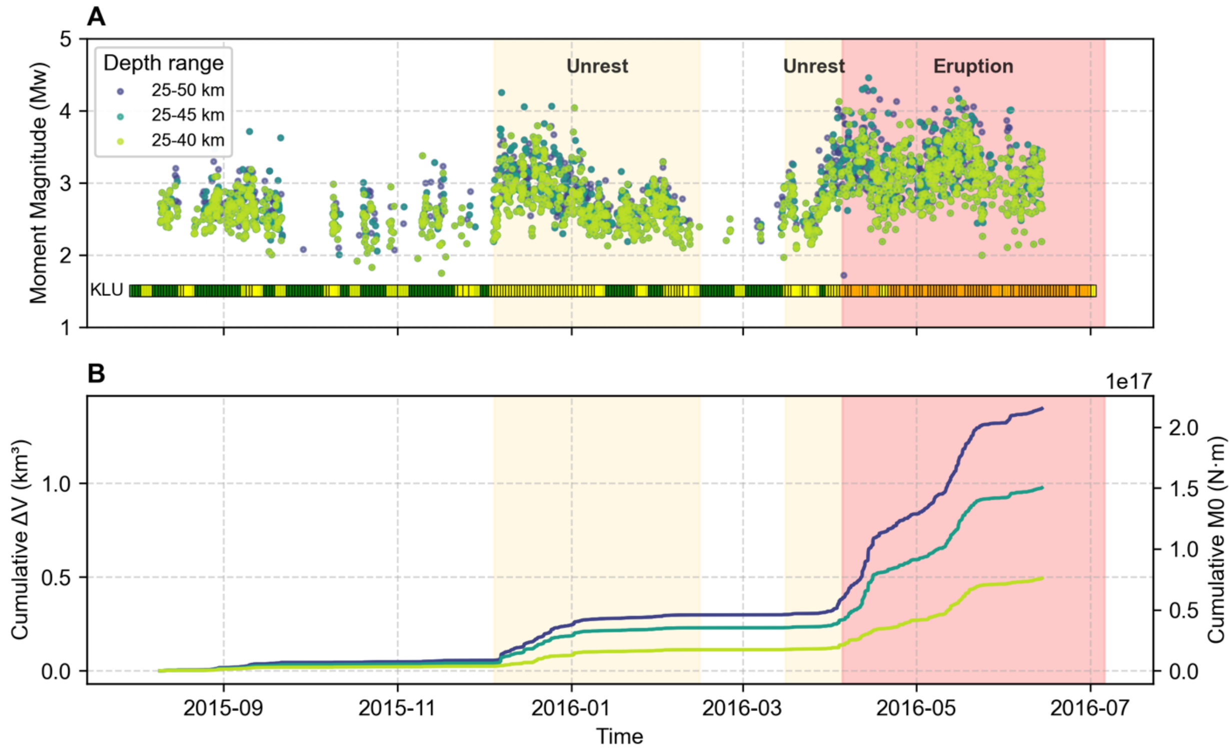

Fig. S5. Time dependent magma influx from the mantle $Q_{tot}(t)$ estimated from seismic tremors considering different source-depth ranges. (A) Moment magnitudes (M_w) of individual tremor events versus time. The horizontal color-coded bar at the bottom tracks the activity status of the Klyuchevskoy (KLU) volcano over the study period (*56,57*), where orange indicates an ongoing eruption. Shaded background regions mark periods of volcanic unrest (yellow) and active eruption (red). Different colors of the tremor symbols indicate the selected source-depth ranges. **(B)** Cumulative seismic moment release (M_0, right axis) and corresponding cumulative volume change (ΔV, left axis) estimated based on equation (6).

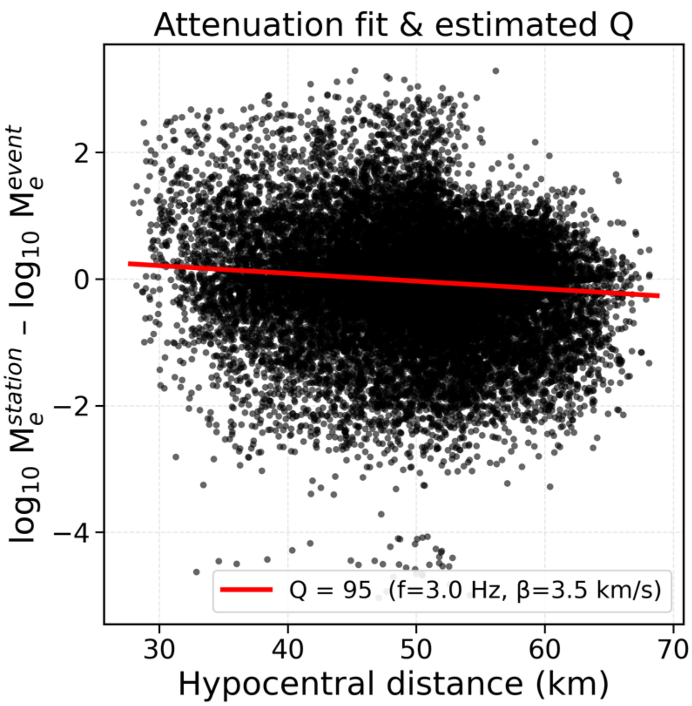

Fig S6. Estimation of inelastic attenuation and quality factor Q. Each point represents a station–event observation of the normalized seismic moment residual. The red line shows the robust linear attenuation fit, yielding $Q = 95$ for f=3 Hz and β=3.5 km/s.

Table S1. Parameter combinations used to assess the uncertainty of the estimated cumulative magma volume.

Parameter	Symbol	SI Unit	This study	C1	C2	C3	C4	C5	C6	C7	C8	C9
Density	ρ	kg/m^3	2830	2830	2830	2500	2830	2830	2830	2830	2830	2830
Shear-wave velocity	β	m/s	3500	3500	3500	3300	3500	3500	3500	3500	3500	3500
Quality factor	Q	-	95	95	95	95	60	130	95	95	95	95
Frequency	f	Hz	3	3	3	3	3	3	1.5	3	3	3
Radiation pattern coefficient	$R_{\theta\phi}$	-	0.72	0.72	0.72	0.72	0.72	0.72	0.72	0.72	0.72	0.72
Free-surface correction factor	F	-	2	2	2	2	2	2	2	2	2	2
window	-	s	5	5	5	5	5	5	5	8	3	5
Depth range	-	km	[25-48.5]	[25-45]	[25-40]	[25-48.5]	[25-48.5]	[25-48.5]	[25-48.5]	[25-48.5]	[25-48.5]	[25-48.5]
medium bulk modulus	K	GPa	100	100	100	100	100	100	100	100	100	50
γ	-	-	650	650	650	650	650	650	650	650	650	650
Cumulative moment	M_0	$N \cdot m$	2.2e+17	1.5e+17	0.8e+17	1.7e+17	4.7e+17	1.5e+17	1.1e+17	3.6e+17	4.4e+17	2.2e+17
Cumulative volume	ΔV	km^3	1.4	1.0	0.5	1.2	3.0	1.0	0.8	2.3	2.9	2.9

C: Combination

REFERENCES

1. B. Black, S. Naif, F. Horton, A. Goltz, C. Wilson, The deep frontier of mantle magma supply. *Eos* **106**, (2025).
2. H. Buurman, M. E. West, J. Power, M. Coombs, Seismic precursors to volcanic explosions during the 2006 eruption of Augustine Volcano. *The* **2006**, 41-57 (2006).
3. J. Claude, J.-C. Mareschal, A. Roman, The Formation of Continental Crust from a Physics Perspective. *Geochem. Int.* **56**, 1289-1321 (2018).
4. J. A. Crisp, Rates of magma emplacement and volcanic output. *Journal of Volcanology and Geothermal Research* **20**, 177-211 (1984).
5. J. O. S. Hammond, J. M. Kendall, Constraints on melt distribution from seismology: a case study in Ethiopia. *Geological Society, London, Special Publications* **420**, 127-147 (2016).
6. C. Magee *et al.*, Magma Plumbing Systems: A Geophysical Perspective. *J. Petrol.* **59**, 1217-1251 (2018).
7. M. Paulatto *et al.*, Advances in seismic imaging of magma and crystal mush. *Front. Earth Sci.* **Volume 10 - 2022**, (2022).
8. O. Bachmann, C. Huber, The volcanic/plutonic ratio in space and time, on Earth and beyond; How efficiently do magmas reach the surface during planetary evolution? *Lithos* **488-489**, 107825 (2024).
9. S. M. White, J. A. Crisp, F. J. Spera, Long-term volumetric eruption rates and magma budgets. *Geochemistry, Geophysics, Geosystems* **7**, (2006).
10. R. A. White, C. Newhall, R. Punongbayan, Precursory deep long-period earthquakes at Mount Pinatubo: Spatio-temporal link to a basalt trigger. *Fire and mud: Eruptions and lahars of Mount Pinatubo, Philippines*, 307-328 (1996).
11. J. A. Power, S. D. Stihler, R. A. White, S. C. Moran, Observations of deep long-period (DLP) seismic events beneath Aleutian arc volcanoes; 1989–2002. *Journal of Volcanology and Geothermal Research* **138**, 243-266 (2004).
12. M. L. Nichols, S. D. Malone, S. C. Moran, W. A. Thelen, J. E. Vidale, Deep long-period earthquakes beneath Washington and Oregon volcanoes. *Journal of Volcanology and Geothermal Research* **200**, 116-128 (2011).
13. N. M. Shapiro *et al.*, Deep and shallow long-period volcanic seismicity linked by fluid-pressure transfer. *Nature Geoscience* **10**, 442-445 (2017b).
14. M. Hensch *et al.*, Deep low-frequency earthquakes reveal ongoing magmatic recharge beneath Laacher See Volcano (Eifel, Germany). *Geophysical Journal International* **216**, 2025-2036 (2019).
15. A. G. Wech, W. A. Thelen, A. M. Thomas, Deep long-period earthquakes generated by second boiling beneath Mauna Kea volcano. *Science* **368**, 775-779 (2020).
16. Z. Song, Y. J. Tan, D. C. Roman, Deep Long-Period Earthquakes at Akutan Volcano From 2005 to 2017 Better Track Magma Influxes Compared to Volcano-Tectonic Earthquakes. *Geophysical Research Letters* **50**, e2022GL101987 (2023).
17. W. Lu, N. M. Shapiro, J. Münchmeyer, Magma Pathways Beneath the Klyuchevskoy Volcanic Group, Kamchatka, Revealed by a Machine-Learning-Based Earthquake Catalog. *Geophysical Research Letters* **53**, e2026GL123629 (2026).
18. R. Kurihara, K. Obara, Spatiotemporal Characteristics of Relocated Deep Low-Frequency Earthquakes Beneath 52 Volcanic Regions in Japan Over an Analysis Period

of 14 Years and 9 Months. *Journal of Geophysical Research: Solid Earth* **126**, e2021JB022173 (2021).
19. N. M. Shapiro, J. Soubestre, C. Journeau, in *Modern Volcano Monitoring,* Z. Spica, C. Caudron, Eds. (Springer Nature Switzerland, Cham, 2025), pp. 107-146.
20. K. Aki, R. Koyanagi, Deep volcanic tremor and magma ascent mechanism under Kilauea, Hawaii. *Journal of Geophysical Research: Solid Earth* **86**, 7095-7109 (1981).
21. C. Journeau *et al.*, Seismic tremor reveals active trans-crustal magmatic system beneath Kamchatka volcanoes. *Science Advances* **8**, eabj1571 (2022).
22. J. Niu, X. Wang, M. Zhang, Q.-F. Chen, J. Jiang, Deep seismic tremor reveals trans-crustal fluid dynamics beneath Tengchong Volcano Field, Southwest China. *Journal of Volcanology and Geothermal Research* **473**, 108577 (2026).
23. N. Aso, V. C. Tsai, Cooling magma model for deep volcanic long-period earthquakes. *Journal of Geophysical Research: Solid Earth* **119**, 8442-8456 (2014).
24. M. Ukawa, M. Ohtake, A monochromatic earthquake suggesting deep-seated magmatic activity beneath the Izu-Ooshima Volcano, Japan. *Journal of Geophysical Research: Solid Earth* **92**, 12649-12663 (1987).
25. O. Melnik, V. Lyakhovsky, N. M. Shapiro, N. Galina, O. Bergal-Kuvikas, Deep long period volcanic earthquakes generated by degassing of volatile-rich basaltic magmas. *Nature Communications* **11**, 3918 (2020).
26. O. Melnik, V. Lyakhovsky, N. M. Shapiro, Rapid Gas Bubble Growth in Basaltic Magma as a Source of Deep Long Period Volcanic Earthquakes. *Journal of Geophysical Research: Solid Earth* **129**, e2024JB029602 (2024).
27. R. White, W. McCausland, Volcano-tectonic earthquakes: A new tool for estimating intrusive volumes and forecasting eruptions. *Journal of Volcanology and Geothermal Research* **309**, 139-155 (2016).
28. T. Ikegaya, M. Yamamoto, Spatio-temporal characteristics and focal mechanisms of deep low-frequency earthquakes beneath the Zao volcano, northeastern Japan. *Journal of Volcanology and Geothermal Research* **417**, 107321 (2021).
29. N. A. Galina, N. M. Shapiro, Source mechanisms of deep long period earthquakes beneath the Klyuchevskoy volcanic group (Kamchatka, Russia) inferred from S-to-P amplitude ratios. *Journal of Volcanology and Geothermal Research* **448**, 108049 (2024).
30. D. Bowers, J. A. Hudson, Defining the scalar moment of a seismic source with a general moment tensor. *Bulletin of the Seismological Society of America* **89**, 1390-1394 (1999).
31. K. Aki, P. G. Richards, *Quantitative Seismology*. (University Science Books, 2002).
32. A. McGarr, Seismic moments and volume changes. *Journal of Geophysical Research (1896-1977)* **81**, 1487-1494 (1976).
33. G. Müller, Volume Change of Seismic Sources from Moment Tensors. *Bulletin of the Seismological Society of America* **91**, 880-884 (2001).
34. K. F. McKee *et al.*, The plausible relationship between deep long-period earthquakes and volatiles: a case study of the Alaska-Aleutian arc. *Bull. Volcanol.* **88**, 115 (2026).
35. N. G. Lensky, R. W. Niebo, J. R. Holloway, V. Lyakhovsky, O. Navon, Bubble nucleation as a trigger for xenolith entrapment in mantle melts. *Earth and Planetary Science Letters* **245**, 278-288 (2006).
36. T. Shea, Bubble nucleation in magmas: A dominantly heterogeneous process? *Journal of Volcanology and Geothermal Research* **343**, 155-170 (2017).

37. O. Roche *et al.*, Shear-induced bubble nucleation in magmas. *Science* **390**, 633-637 (2025).
38. A. N. Clark, C. E. Lesher, Elastic properties of silicate melts: Implications for low velocity zones at the lithosphere-asthenosphere boundary. *Science Advances* **3**, e1701312.
39. N. M. Shapiro *et al.*, Understanding Kamchatka's extraordinary: Volcano Cluster. *EOS: Transactions, American Geophysical Union* **98**, 12-17 (2017a).
40. I. Melekestsev, Volcanism and relief formation. *Science, Moscow (in Russian)*, (1980).
41. S. Auer, I. Bindeman, P. Wallace, V. Ponomareva, M. Portnyagin, The origin of hydrous, high-δ18O voluminous volcanism: diverse oxygen isotope values and high magmatic water contents within the volcanic record of Klyuchevskoy volcano, Kamchatka, Russia. *Contrib. Mineral. Petrol.* **157**, 209-230 (2009).
42. V. Cayol, J. H. Dieterich, A. T. Okamura, A. Miklius, High Magma Storage Rates Before the 1983 Eruption of Kilauea, Hawaii. *Science* **288**, 2343-2346 (2000).
43. N. M. Shapiro, A. V. Gorbatov, E. Gordeev, J. Dominguez, Average shear-wave velocity structure of the Kamchatka peninsula from the dispersion of surface waves. *Earth, Planets and Space* **52**, 573-577 (2000).
44. S. Senyukov, Forecasting of the eruptions of volcanoes Klyuchevskoy and Bezymianny at Kamchatka. *Lambert Academic*, (2013).
45. D. V. Droznin *et al.*, Detecting and locating volcanic tremors on the Klyuchevskoy group of volcanoes (Kamchatka) based on correlations of continuous seismic records. *Geophysical Journal International* **203**, 1001-1010 (2015).
46. V. Levin, S. Droznina, M. Gavrilenko, M. J. Carr, S. Senyukov, Seismically active subcrustal magma source of the Klyuchevskoy volcano in Kamchatka, Russia. *Geology* **42**, 983-986 (2014).
47. N. Shapiro *et al.*, Klyuchevskoy volcanic group experiment (KISS). (2015).
48. T. C. Hanks, H. Kanamori, A moment magnitude scale. *Journal of Geophysical Research: Solid Earth* **84**, 2348-2350 (1979).
49. N. A. Galina *et al.*, Recurrence of Deep Long-Period Earthquakes beneath the Klyuchevskoi Volcano Group, Kamchatka. *Izvestiya, Physics of the Solid Earth* **56**, 749-761 (2020).
50. H. Kao, K. Wang, H. Dragert, J. Y. Kao, G. Rogers, Estimating seismic moment magnitude (Mw) of tremor bursts in northern Cascadia: Implications for the "seismic efficiency" of episodic tremor and slip. *Geophysical Research Letters* **37**, (2010).
51. J. B. Fletcher, A. McGarr, Moments, magnitudes, and radiated energies of non-volcanic tremor near Cholame, CA, from ground motion spectra at UPSAR. *Geophysical Research Letters* **38**, (2011).
52. S. M. Plank *et al.*, Estimates of lava discharge rate of 2018 Kīlauea Volcano, Hawaiʻi eruption using multi-sensor satellite and laboratory measurements. *Int. J. Remote Sens.* **42**, 1492 - 1511 (2021).
53. D. Coppola *et al.*, Thermal remote sensing reveals communication between volcanoes of the Klyuchevskoy Volcanic Group. *Scientific Reports* **11**, 13090 (2021).
54. A. Campus *et al.*, Effusion Rate Trends at Piton de la Fournaise: A Review of 24 Years of Space-Based Thermal Observation. *Journal of Geophysical Research: Solid Earth* **130**, e2024JB030962 (2025).
55. Kamchatka Branch of the Geophysical Survey of the Russian Academy of Sciences. (1961).

56. Daily activity level color codes for Kamchatka volcanoes (in Russian): www.emsd.ru/ssl/monitoring/main.htm/.
57. S. L. Senyukov, D. V. Droznin, I. N. Nuzhdina, S. Y. Droznina, The Twenty Five Years of “Volcanic Activity Monitoring”—Observations and Results. *J. Volcanol. Seismolog.* **20**, 284-304 (2026).
58. L. Seydoux, N. M. Shapiro, J. de Rosny, F. Brenguier, M. Landès, Detecting seismic activity with a covariance matrix analysis of data recorded on seismic arrays. *Geophysical Journal International* **204**, 1430-1442 (2016).
59. J. Soubestre *et al.*, Depth Migration of Seismovolcanic Tremor Sources Below the Klyuchevskoy Volcanic Group (Kamchatka) Determined From a Network-Based Analysis. *Geophysical Research Letters* **46**, 8018-8030 (2019).
60. C. Journeau *et al.*, Detection, Classification, and Location of Seismovolcanic Signals with Multicomponent Seismic Data: Example from the Piton de La Fournaise Volcano (La Réunion, France). *Journal of Geophysical Research: Solid Earth* **125**, e2019JB019333 (2020).
61. F. Tong, L. Seydoux, C. Journeau, J. Soubestre. Covseisnet/covseisnet: Associate repository with a zenodo (Zenodo, 2024). https://doi.org/10.5281/zenodo.10990031
62. N. I. Christensen, W. D. Mooney, Seismic velocity structure and composition of the continental crust: A global view. *Journal of Geophysical Research: Solid Earth* **100**, 9761-9788 (1995).
63. V. Levin, S. Droznina, M. Gavrilenko, M. J. Carr, S. Senyukov, Seismically active subcrustal magma source of the Klyuchevskoy volcano in Kamchatka, Russia. *Geology* **42**, 983-986 (2014).
64. S. Y. Droznina *et al.*, S-wave velocity model for several regions of the Kamchatka Peninsula from the cross correlations of ambient seismic noise. *Izvestiya, Physics of the Solid Earth* **53**, 341-352 (2017).
65. G. Kwiatek, Y. Ben-Zion, Assessment of P and S wave energy radiated from very small shear-tensile seismic events in a deep South African mine. *Journal of Geophysical Research: Solid Earth* **118**, 3630-3641 (2013).